ARTICLE   OPEN

Check for updates

Antinodal kink in the band dispersion of electron-doped cuprate La$_{2-x}$Ce$_x$CuO$_{4\pm\delta}$

C. Y. Tang [1,2,7], Z. F. Lin [1,2,7], J. X. Zhang[3], X. C. Guo[1,2], Y. G. Zhong[1,2], J. Y. Guan[1,2], S. Y. Gao[1,2], Z. C. Rao[1,2], J. Zhao[1,2], Y. B. Huang [4], T. Qian [1,5], Z. Y. Weng[3], K. Jin [1,2,5 ✉], Y. J. Sun [1,6 ✉] and H. Ding [1,2,5 ✉]

Angle-resolved photoemission spectroscopy (ARPES) measurements have established the phenomenon of kink in band dispersion of high-T_c cuprate superconductors. However, systematic studies of the kink in electron-doped cuprates are still lacking experimentally. We performed in situ ARPES measurements on La$_{2-x}$Ce$_x$CuO$_{4\pm\delta}$ (LCCO) thin films over a wide electron doping (n) range from 0.05 to 0.23. While the nodal kink is nearly invisible, an antinodal kink around 45 meV, surviving above 200 K, is observed for $n \sim 0.05$–0.19, whose position is roughly independent of doping. The fact that the antinodal kink observed at high temperatures and in the highly overdoped region favors the phonon mechanism with contributions from the Cu–O bond-stretching mode and the out-of-plane oxygen buckling mode.

INTRODUCTION

The kink phenomenon in cuprates, as a sudden change in the slope of band dispersion revealed by angle-resolved photoemission spectroscopy (ARPES), remains unsolved and intriguing[1–3]. The kink is also indirectly revealed in inelastic neutron scattering (INS), inelastic X-ray scattering (IXS), Raman, and optical measurements as an anomaly in the density of states or intensities[4–7]. However, despite decades of extensive studies, the origin of kink remains controversial, electron-boson coupling (EBC), spin fluctuations, and spin-charge separation have been suggested as possible causes[2,8–10]. Among them, EBC is arguably the most preferred mechanism, with phonons, magnetic resonance modes, and polarons serving as potential candidates for the bosonic mode[11–13]. Since the electron-phonon coupling is generally regarded as the pairing glue in conventional superconductors, the bosonic mode referred from the kink in the cuprates is widely argued to play a significant role in the high-T_c superconductivity.

In the most extensively studied cuprates Bi$_2$Sr$_2$CaCu$_2$O$_{8+\delta}$ (BSCCO) and Bi$_2$Sr$_{1.6}$La$_{0.4}$CuO$_{6+\delta}$, ARPES data display a strong kink with the binding energy of ~70 meV along the nodal direction and a weaker kink around ~40 meV near the antinode[5,14,15]. While the antinodal kink is widely believed to be related to the magnetic resonance mode or the oxygen buckling mode (out-of-plane oxygen O2 moves parallel to the c-axis, B_{1g} mode)[5,12], the nodal kink is more complicated[5,10,16,17]. In La$_{2-x}$Sr$_x$CuO$_4$, benefited from the large sample size, both ARPES and INS experiments can be performed. The nodal kink appears in LSCO at the metal-insulator transition, which is interpreted as the Cu–O bond-stretching mode (also known as the breathing mode, E_u mode) or polaron mode[4,13,18]. In electron-doped cuprates Nd$_{1.85}$Ce$_{0.15}$CuO$_{4\pm\delta}$ (NCCO), Sm$_{1.85}$Ce$_{0.15}$CuO$_{4\pm\delta}$ (SCCO), and Eu$_{1.85}$Ce$_{0.15}$CuO$_{4\pm\delta}$ (ECCO), ARPES experiments suggest that the antinodal photo-hole couples to full-breathing phonons ($q = [0.5, 0.5, 0]$, 70 meV), and the nodal photo-hole couples to half-breathing phonons ($q = [0.5, 0, 0]$, 50 meV)[19]. The significant phonon softening along the [100] direction in many cuprates is discovered by the INS measurements[20]. Although the kink seems universal in the hole-doped and electron-doped cuprates, systematic studies of doping and temperature dependence of the kink in electron-doped cuprates are still lacking. Especially, there are no ARPES results for the kink effect in La$_{2-x}$Ce$_x$CuO$_{4\pm\delta}$ (LCCO), which has the largest rare-earth ion radius and the highest T_c among the electron-doped cuprates. Motivated by this, we prepared high-quality LCCO films by the elaborate ozone/vacuum annealing method[21], and conducted ARPES measurements to systematically study the kink effect in this material.

RESULTS

Antinodal kink

We plot the doping evolution of the band structures of LCCO in Fig. 1. Figure 1a, b displays the band dispersions near the node and antinode with the electron doping level (n) varies from $n \sim$ 0.05 to $n \sim$0.23, respectively. The black lines are the band dispersions extracted from the momentum distribution curves (MDCs) by Lorentzian fitting, and the red lines are the assumed linear bare bands. The kink displays itself as a discrepancy between those two lines. It is clear that the kink is indiscernible in the nodal region, but it is ever-existing near the antinode, except for the heavily overdoped sample with $n \sim 0.23$. While in the hole-doped LSCO, the kink is more conspicuous along the nodal direction[8]. To get a better view, we show the second derivative images of the band dispersions at $n \sim 0.084$ in Fig. 1d. The dashed white lines indicate the antiferromagnetic (AF) zone boundary (AFZB), where the nodal band shows a band-folding behavior with no existence of kink (cut 1). While the AF gap locates at the AFZB at the near hotspot (cut 2), the kink position at the antinode (cut 3) is away from it, which resembles the case in NCCO[22].

In general, ARPES probes the single-particle spectral function directly, and the many-body interactions exhibiting themselves as

[1]Beijing National Laboratory for Condensed Matter Physics and Institute of Physics, Chinese Academy of Sciences, 100190 Beijing, China. [2]University of Chinese Academy of Sciences, 100049 Beijing, China. [3]Institute for Advanced Study, Tsinghua University, 100084 Beijing, China. [4]Shanghai Advanced Research Institute, Chinese Academy of Sciences, 201204 Shanghai, China. [5]Songshan Lake Materials Laboratory, 523808 Dongguan, Guangdong, China. [6]Department of Physics, Southern University of Science and Technology, 518055 Shenzhen, China. [7]These authors contributed equally: C. Y. Tang, Z. F. Lin. ✉email: kuijin@iphy.ac.cn; sunyj@sustech.edu.cn; dingh@iphy.ac.cn
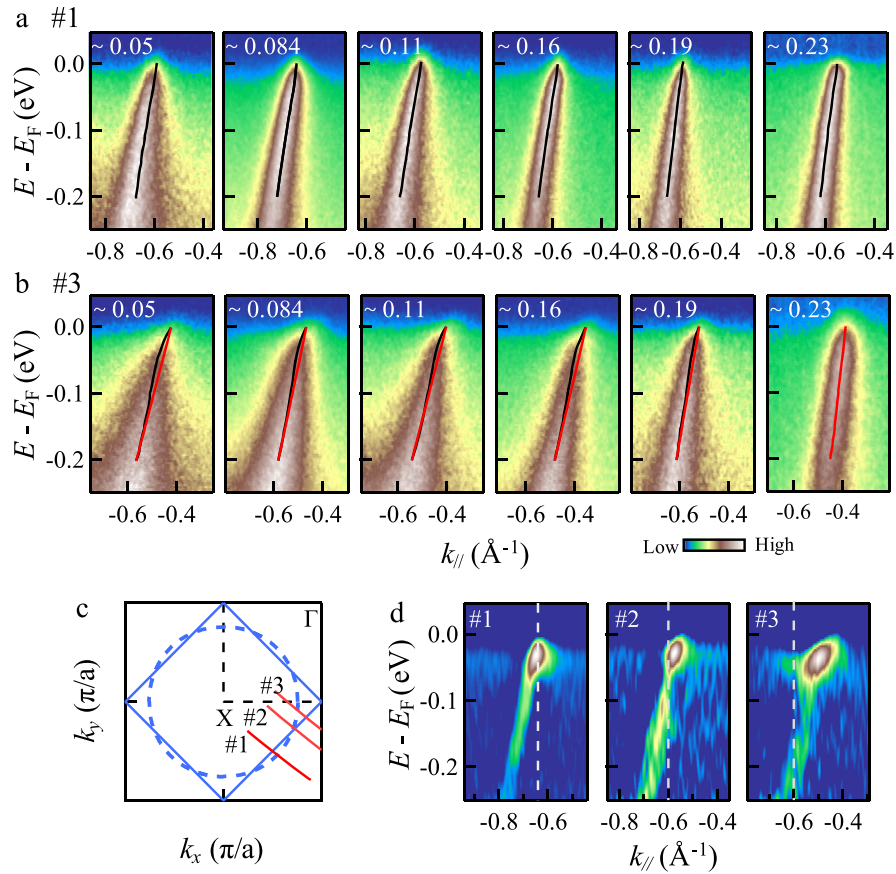
Fig. 1 Band dispersions in LCCO. a Nodal band dispersion of LCCO for $n \sim 0.05-0.23$. The momentum position of these bands is indicated as cut 1 in **c**. ARPES spectrum at the node of $n \sim 0.084$ was performed at 10 K. **b** Band dispersion near the antinode, represented as cut 3 in **c**. For $n \sim 0.05-0.11$, samples were ozone/vacuum annealed from as-grown films with Ce concentration $x = 0.1$, and for $n \sim 0.14-0.19$, samples were annealed from one film with $x = 0.19$. The band structures at $n \sim 0.23$ are from our previous work[21]. The black lines are the peaks of the MDCs extracted by Lorentzian fitting, and the red lines are the assumed linear bare bands. **c** Schematic of the Fermi surface at $n \sim 0.084$. Cut 1, cut 2, and cut 3 indicate the momentum cuts along the nodal direction, the near hotspot, and the antinode. **d** Second derivative images of the band dispersions at $n \sim 0.084$ as marked in **c**. The white dashed lines indicate the antiferromagnetic zone boundary.
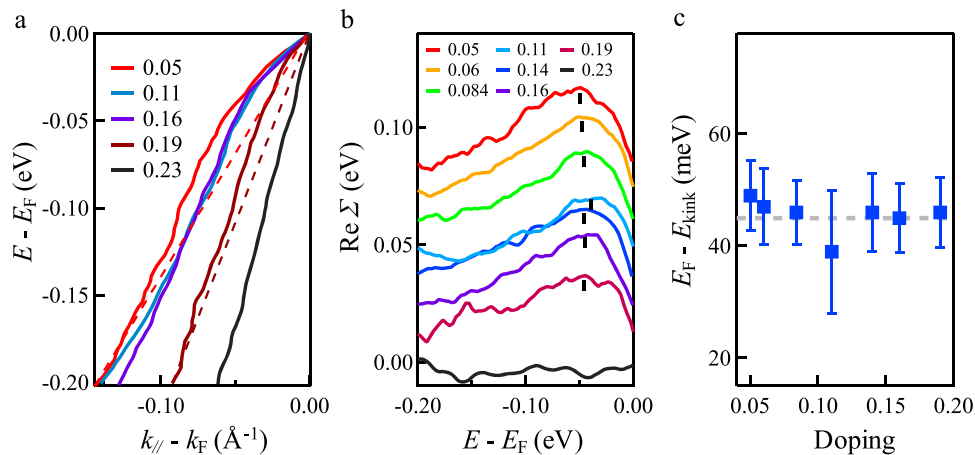

Fig. 2 Universal antinodal kink in LCCO. a MDC-derived antinodal band dispersions at different doping levels are displayed as the solid lines, and the dashed lines represent the linear bare bands connecting the E_F to $E_F -200$ meV. **b** Extracted real part of the self-energies, the curves are offset vertically for clarity. **c** Doping dependence of the peak position of Re Σ, the mean energy of the kink is at ~ 45 meV. Error bars are the overestimated uncertainty of determining the peak positions.

renormalization effects in band dispersion are included in the self-energy. The peak position of the real part of self-energy (Re Σ) corresponds to the characteristic energy of the kink. We extract the antinodal band dispersions as shown in Fig. 2a and plot the Re

Σ versus $E - E_F$ in Fig. 2b, where the curves are offset vertically for clarity. It is clear that except at $n \sim 0.23$, all the samples indicate a kink at 40–50 meV, with the mean energy at ~ 45 meV, as summarized in Fig. 2c. In the underdoped region below 0.11, the
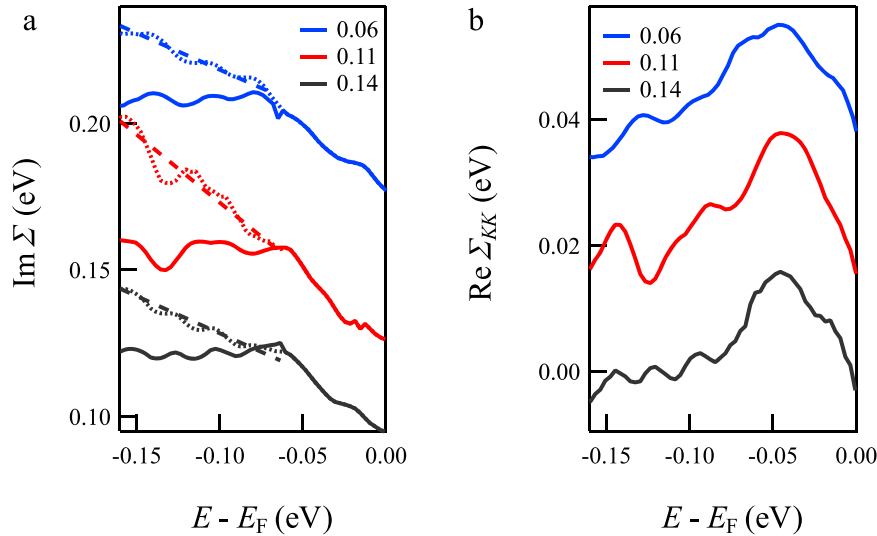
Fig. 3 Imaginary part of self-energy. a Imaginary parts of self-energies (Im Σ) of the antinodal data in Figs. 1 and 2 for $n \sim 0.06$ (underdoped), 0.11 (optimally doped), and 0.14 (overdoped) are presented in dotted lines. The solid lines represent the boson contribution to Im Σ after a linear background (dashed lines) is subtracted. **b** Re Σ_{KK} as the Kramers-Kronig transformation of the boson contribution to Im Σ in **a**. For both panels, data are shifted vertically for ease of view.

kink shows energy softening with the increasing electron doping level, which may be related to the Coulomb screening of the increasing free charge carriers. The characteristic energy slightly increases in the overdoped region, possibly due to the less effective screening or the interaction with the O2 branch[20,23]. We shall clarify that the kink energy is the sum of the bosonic coupling energy and the superconducting gap energy, while the influence of the superconducting gap is neglected in our work[24–26]. The superconducting gap in the electron-doped cuprates is relatively small, which is below our energy resolution and thus will not cause any meaningful difference to our conclusion[27–29].

Imaginary part
To gain more insight into the kink phenomena, we introduce the imaginary part of self-energy (Im Σ) along the antinodal direction for $n \sim 0.06$, 0.11, and 0.14 in Fig. 3a. The dotted lines in Fig. 3a show a considerable slope change around 45 meV. Electron-boson coupling, electron–electron interactions, and impurity scattering are all identified mechanisms responsible for the finite lifetime of a photo-hole[30]. The electron–electron interaction is approximately linear above the kink energy, and we subtract the linear background to obtain the boson contribution (solid lines)[19,31]. As shown in Fig. 3b, by the Kramers-Kronig relation, the Re Σ_{KK} has a peak at ~ 45 meV, where the boson contribution to Im Σ has a steplike feature. The similar lineshape between the Re Σ and Re Σ_{KK} further supports the existence of the antinodal kink. The rest of the dataset is shown in Supplementary Fig. 1.

There are several ways to estimate the EBC strength. For $n \sim 0.11$, the band velocity is renormalized from $v_F^0 = 1.6$ eVÅ^{-1} to $v_F = 0.95$ eVÅ^{-1}. Conventionally, the EBC constant is obtained as $\lambda = v_F^0/v_F - 1 \sim 0.7$. One can also estimate the EBC strength from the real part of self-energy to be $\lambda = -\frac{dRe\Sigma(E)}{dE}\Big|_{E=E_F} \sim 0.9$ at $n \sim 0.11$[32]. According to the Eliashberg formula, the electron-boson spectral function $\alpha^2 F(\omega, k)$ is obtained by the derivative of Im Σ, as seen in Supplementary Fig. 2 for $n \sim 0.11$. The coupling strength $\lambda(\epsilon, k) = 2\int_0^{\omega_{max}} \alpha^2 F(\omega, k; \epsilon)/\omega d\omega$ is calculated to be $\lambda \sim 0.7$ for $n \sim 0.11$, where ω_{max} is the maximum phonon energy[32,33]. Therefore, we summarized that in the optimally doped LCCO, the EBC strength is about 0.8 ± 0.2. In the optimally doped NCCO, SCCO, and Bi2212 along the nodal direction, the coupling constant is estimated to be $\lambda \sim 0.8$[19,34].

Temperature dependence of the kink
To get more information on this kink effect, we performed temperature-dependent ARPES experiments in the antinodal region of LCCO and plotted Re Σ at different temperatures in Fig. 4a, b. The electron doping levels are estimated to be $n \sim 0.084$ and 0.175, which lies in the underdoped and the highly overdoped region of the superconducting dome of LCCO, respectively[35]. For $n \sim 0.084$, the peak positions of Re Σ stay at similar energies, which are represented as the red dots in Fig. 4c, and the kink survives at $T = 200$ K. Meanwhile, Re Σ shows a two-peak structure at around 30 meV and 70 meV at 120 K, indicating a possibility that the antinodal region may consist of two electron-boson couplings. Within the commonly used Eliashberg-type electron-boson coupling model, there is a softening of the kink at high temperatures due to the finite temperature quantum statistics. While the softening is expected in order of a few meV, it is beyond the energy resolution in the current study[2,25,31,34]. The case is the same in the overdoped region at $n \sim 0.175$. For quantitative analysis, we calculate the spectral weight of Re Σ by integrating over E_F to $E_F -200$ meV and show the results in Fig. 4d. This sum area includes all the disparity between the bare band and renormalized band above -200 meV. Extracted using a linear bare band, the sum area of Re Σ is a reasonable way to comparatively estimate the contribution of bosonic modes below 200 meV to the real part of self-energy. For comparison, we also extract the spectral weight of Re Σ in the nodal region of BSCCO and LSCO[8,10]. The result suggests that the antinodal renormalization in LCCO is comparable to the renormalization effect along the nodal direction in the hole-doped cuprates. The magnitude of Re Σ decreases slowly with increasing temperature, and its energy shows little doping dependence, resembling the behavior in the hole-doped cuprates[11,36,37].

Comparison of the kinks for different cuprates
To advance our understanding of the antinodal kink in LCCO, we plot and compare the energy scales of the kinks in different cuprate systems in Fig. 5. In the hole-doped cuprate BSCCO, the nodal kink stays at ~ 70 meV, and the antinodal region shows a kink feature at ~ 40 meV[14]. It has been interpreted as the parallel and isotropic shifts of multiple kinks[26]. While the antinodal kink is not prominent, combined ARPES and INS data have shown

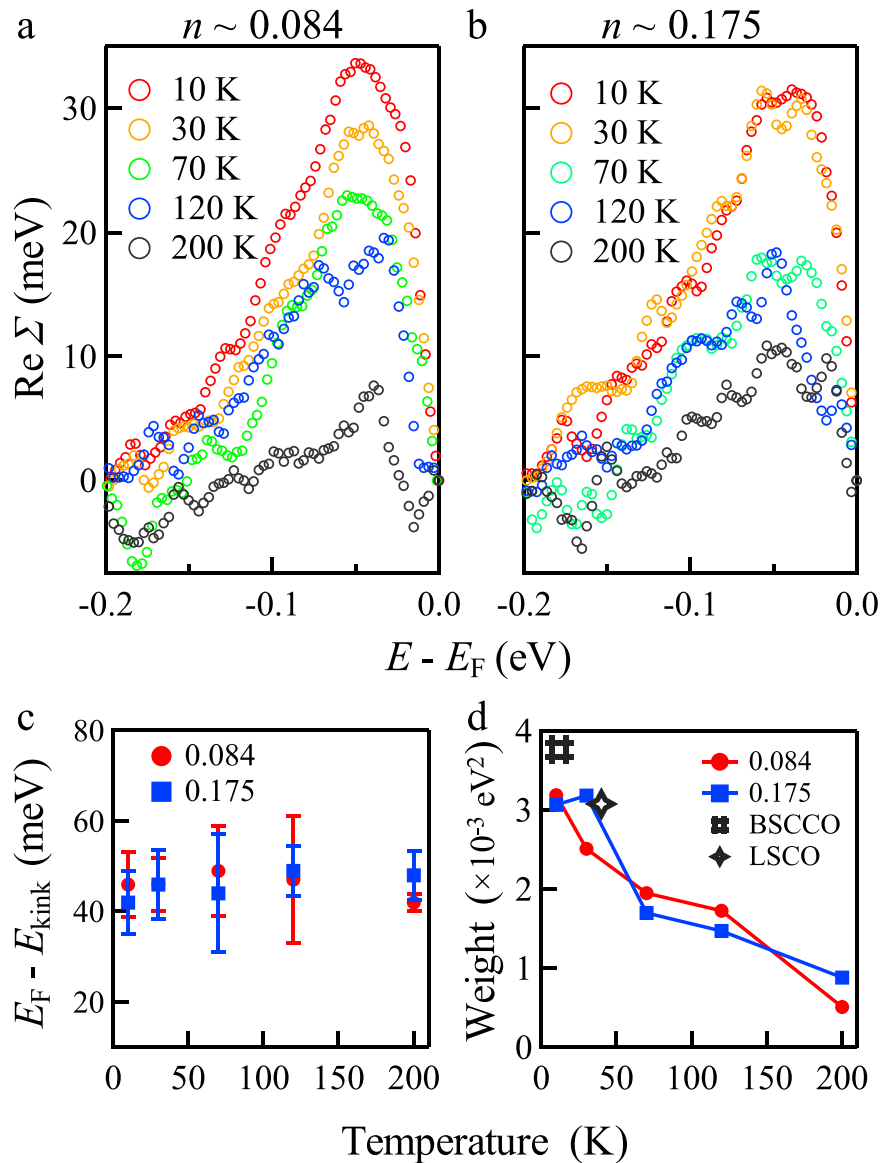**Fig. 4 Temperature dependence of the antinodal kink. a, b** Temperature dependence of the real part of self-energy for $n \sim 0.084$, 0.175 along the antinodal direction, respectively. The sample at $n \sim 0.175$ was ozone/vacuum annealed from an as-grown film with Ce concentration $x = 0.15$. **c** Extracted peak positions of the Re Σ for $n \sim 0.084$ (red dots) and 0.175 (blue squares) at different temperatures. Error bars are the overestimated uncertainty of determining the peak positions. **d** Spectral weight of Re Σ by integrating over E_F to E_F −200 meV for $n \sim 0.084$ and 0.175. The spectral weight of BSCCO and LSCO are presented for comparison. Both cases assume a linear bare band, but the Re Σ in BSCCO is limited in an energy range below 180 meV.

a ~ 70 meV in the nodal region of LSCO[4,18]. In electron-doped cuprates NCCO, SCCO, and ECCO, the 70 meV kink near the antinode is regarded as the Cu–O bond full-breathing mode[19]. Along the nodal direction, the 50 meV kink detected in NCCO and SCCO is related to the Cu–O bond half-breathing mode. In LCCO with the largest La^{3+} ion radius among the lanthanide elements, besides the disappearance of the nodal kink, the antinodal kink alters to ~ 45 meV, which is downshifted from the antinodal kink energy in other electron-doped cuprates at ~ 70 meV.

DISCUSSION

We now try to understand the origin of this universal kink in the antinodal region in LCCO. There are several candidates with a possible origins. First of all, the widely debated magnetic resonance mode in the hole-doped cuprates is unlikely to explain the antinodal kink in LCCO. While the magnetic resonance mode

in the hole-doped cuprates is around 40 meV[12,38], it is found to be ~ 10 meV in the electron-doped cuprates by neutron scattering[39,40], and this energy scale is much smaller than the observed kink energy at ~ 45 meV.

Second, some previous work pointed out that the antinodal kink in the electron-doped cuprates may originate from the opening of the AF gap[3,41,42]. We rule out this assumption for the following reasons: (1) the momentum position where the renormalization happens is away from the AFZB, as seen in Fig. 1c; (2) in the overdoped region $n \sim 0.14$–0.19 where the AF fluctuations have vanished, the kink effect remains strong. And this kink is robust at $n \sim 0.15$ at 200 K, suggesting that the proximity to the AF gap is not the mechanism.

Next, we turn to the extensively studied phonon modes. By comparing the energy scales, we found that the typical energy of the B_{1g} mode is at ~ 40 meV and the Cu–O bond-stretching mode is at ~ 40–70 meV, which is close to the kink we observed
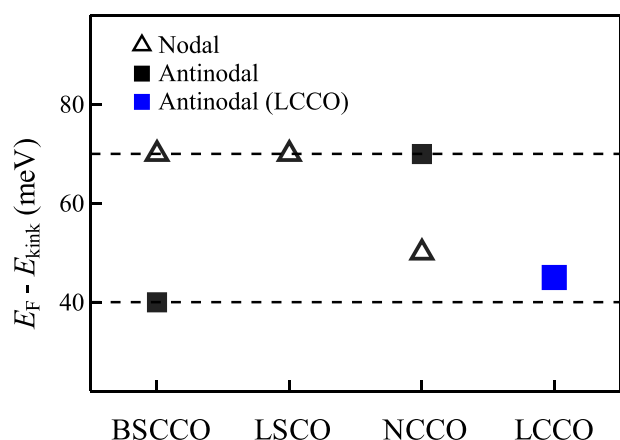
Fig. 5 Comparison of the kink energies. The energy scales of the kinks along the nodal direction (empty triangle symbols) and near the antinodal region (solid square symbols) in the hole- and electron-doped cuprates. The dashed lines at 40 and 70 meV represent the characteristic energies of the kinks. In LCCO, the nodal kink is disappeared, but the antinode has a universal kink at ~ 45 meV (indicated as the blue square).

at ~ 45 meV. The 70 meV kink near the antinode of NCCO, SCCO, and ECCO revealed by ARPES and INS experiments has been assigned to the oxygen full-breathing mode. Since the breathing mode is infrared-active, an optical measurement in $Pr_{1.85}Ce_{0.15}CuO_{4\pm\delta}$ (PCCO) with the E_u peak at ~ 50 meV supports the mechanism of the Cu–O bond-stretching mode[43]. Besides, the B_{1g} mode is Raman-active and has been confirmed in PCCO, NCCO, SCCO, and $Gd_{1.85}Ce_{0.15}CuO_{4\pm\delta}$ (GCCO) by Raman experiments[6]. A mode at $308.5 cm^{-1}$ (~ 38 meV) observed in LCCO is likely ascribed to the B_{1g} mode[44]. Moreover, the mode energy decreases continuously with increasing rare-earth radius, which is consistent with our data. All these results imply that the kink observed in the antinodal region in LCCO may be attributed to the B_{1g} and E_u phonon modes.

However, there are still some concerns. Firstly, we suggest a phonon origin based on the features of the kink, for its existence in the highly overdoped region and high temperatures. But the specific phonon mode is an assumption considering the similar energy scales. More experiments like Raman, optical, and INS in LCCO are needed to provide confirming information, though the last one may be difficult to perform due to the thin-film form.

Moreover, the kink along the nodal direction is inconspicuous in LCCO and not prominent in NCCO/SCCO compared to that near the antinode. This behavior has a huge difference from the hole-doped cuprates, where the nodal kink is strong and holds some anomalous characteristics. Recent works have proposed an idea by assigning the anomalously nodal kink in BSCCO to the spin-charge separation[10,45]. It was suggested that quasiparticle excitations maintain coherence within the Fermi pocket, and electrons with higher binding energies than the energy of the kink decay into spinons and holons, causing the abrupt change of the bandwidth. At the antinodal region of LCCO, the decay of the quasiparticles is likely processed by phonon emission that causes the line broadening, while the nodal band dispersion remains sharp. Since the antinodal region seems conventional in LCCO, the nodal region may embody intrinsic physics, like the high-T_c superconductivity and the electron-hole symmetry/asymmetry. Is there any relation between the dichotomy of the nodal and antinodal region in the hole- and electron-doped cuprates? Is the kink influenced by the distance to the cross point of AFZB and Fermi surface? What mechanisms may be concealed in the linear-like nodal band dispersion and the much smaller superconducting

gap in LCCO? To answer these questions, further studies are needed.

In summary, we have observed a universal kink at ~ 45 meV in the antinodal region of LCCO, the energy scale of which is roughly doping-independent and temperature-independent. We attribute the kink to the Cu–O bond full-breathing mode and the out-of-plane oxygen buckling mode by comparing the kink energy and considering the results in other electron-doped cuprates. It implies that phonon modes are universal in both hole- and electron-doped cuprates.

METHODS
Samples and ARPES measurements
High-quality LCCO thin films were grown by pulsed laser deposition (PLD) with Ce concentrations $x = 0.1$, 0.15, and 0.19. The electron doping level, determined by oxygen and Ce stoichiometry, is estimated by fitting the Fermi surface volume using the tight-binding model. By the two-step ozone/vacuum annealing method described previously, we were able to measure ARPES spectra on LCCO films from $n \sim 0.05$ to 0.23[21]. For $n \sim$ 0.05–0.19, we performed ARPES measurements with a Scienta R4000 analyzer and a VUV helium light source. He-IIα resonant line (40.8 eV) was used and the base pressure of the ARPES system is at ~ 4×10^{-11} torr. To ensure that the samples at all doping levels are in the normal state, all measurements were carried out at 30 K, unless otherwise specified. For $n \sim$ 0.23, ARPES spectrum was measured at the Dreamline beamline of the Shanghai Synchrotron Radiation Facility (SSRF) with a Scienta Omicron DA30L analyzer at ~ 20 K, with the photon energy of 55 eV. The experiments were performed with an energy resolution of ~ 30 meV.

DATA AVAILABILITY
Data are available from the corresponding author upon reasonable request.

REFERENCES
1. Sobota, J. A., He, Y. & Shen, Z. X. Angle-resolved photoemission studies of quantum materials. *Rev. Mod. Phys.* **93**, 1–72 (2021).
2. Li, Z., Wu, M., Chan, Y. H. & Louie, S. G. Unmasking the origin of kinks in the photoemission spectra of cuprate superconductors. *Phys. Rev. Lett.* **126**, 146401 (2021).
3. Armitage, N. P., Fournier, P. & Greene, R. L. Progress and perspectives on electron-doped cuprates. *Rev. Mod. Phys.* **82**, 2421–2487 (2010).
4. McQueeney, R. J., Sarrao, J. L., Pagliuso, P. G., Stephens, P. W. & Osborn, R. Mixed lattice and electronic states in high-temperature superconductors. *Phys. Rev. Lett.* **87**, 077001 (2001).
5. Graf, J. et al. Bond stretching phonon softening and kinks in the angle-resolved photoemission spectra of optimally doped $Bi_2Sr_{1.6}La_{0.4}Cu_2O_{6+\delta}$ superconductors. *Phys. Rev. Lett.* **100**, 227002 (2008).
6. Heyen, E. T. et al. Phonon anomalies and structural stability in the $R_{2-x}Ce_xCuO_4$ system (R = Gd, Sm, Nd, Pr). *Phys. Rev. B* **43**, 2857 (1991).
7. Homes, C. C., Clayman, B. P., Peng, J. L. & Greene, R. L. Optical properties of $Nd_{1.85}Ce_{0.15}CuO_4$. *Phys. Rev. B* **56**, 5525 (1997).
8. Park, S. R. et al. Broken relationship between superconducting pairing interaction and electronic dispersion kinks in $La_{2-x}Sr_xCuO_4$ measured by angle-resolved photoemission. *Phys. Rev. B* **88**, 220503(R) (2013).
9. Dahm, T. et al. Strength of the spin-fluctuation-mediated pairing interaction in a high-temperature superconductor. *Nat. Phys.* **5**, 217–221 (2009).
10. Zhong, Y. et al. Anomalous doping evolution of nodal dispersion revealed by in situ ARPES on continuously doped cuprates. *Phys. Rev. B* **100**, 184504 (2019).
11. Lanzara, A. et al. Evidence for ubiquitous strong electron-phonon coupling in high-temperature superconductors. *Nature* **412**, 510–514 (2001).
12. Fong, H. F. et al. Neutron scattering from magnetic excitations in $Bi_2Sr_2CaCu_2O_{8+\delta}$. *Nature* **398**, 588–591 (1999).
13. Mishchenko, A. S. et al. Polaronic metal in lightly doped high-T_c cuprates. *EPL* **95**, 57007 (2011).
14. He, J. et al. Coexistence of two sharp-mode couplings and their unusual momentum dependence in the superconducting state of $Bi_2Sr_2CaCu_2O_{8+\delta}$

revealed by laser-based angle-resolved photoemission. *Phys. Rev. Lett.* **111**, 107005 (2013).

15. Van Heumen, E., Meevasana, W., Kuzmenko, A. B., Eisaki, H. & Van Der Marel, D. Doping-dependent optical properties of Bi2201. *N. J. Phys.* **11**, 055067 (2009).

16. Matsuyama, K., Perepelitsky, E. & Shastry, B. S. Origin of kinks in the energy dispersion of strongly correlated matter. *Phys. Rev. B* **95**, 165435 (2017).

17. Devereaux, T. P., Cuk, T., Shen, Z. X. & Nagaosa, N. Anisotropic electron-phonon interaction in the cuprates. *Phys. Rev. Lett.* **93**, 117004 (2004).

18. Zhou, X. J. et al. Universal nodal Fermi velocity. *Nature* **423**, 398–398 (2003).

19. Park, S. R. et al. Angle-resolved photoemission spectroscopy of electron-doped cuprate superconductors: Isotropic electron-phonon coupling. *Phys. Rev. Lett.* **101**, 117006 (2008).

20. Braden, M., Pintschovius, L., Uefuji, T. & Yamada, K. Dispersion of the high-energy phonon modes in $Nd_{1.85}Ce_{0.15}CuO_4$. *Phys. Rev. B* **72**, 184517 (2005).

21. Tang, C. Y. et al. Suppression of antiferromagnetic order in the electron-doped cuprate T'-$La_{2-x}Ce_xCuO_{4\pm\delta}$. *Phys. Rev. B* **104**, 155125 (2021).

22. He, J. et al. Fermi surface reconstruction in electron-doped cuprates without antiferromagnetic long-range order. *Proc. Natl Acad. Sci. USA* **116**, 3449–3453 (2019).

23. Meevasana, W. et al. Doping dependence of the coupling of electrons to bosonic modes in the single-layer high-temperature $Bi_2Sr_2CuO_6$ superconductor. *Phys. Rev. Lett.* **96**, 157003 (2006).

24. Lee, W. S., Johnston, S., Devereaux, T. P. & Shen, Z. X. Aspects of electron-phonon self-energy revealed from angle-resolved photoemission spectroscopy. *Phys. Rev. B* **75**, 195116 (2007).

25. Lee, W. S. et al. Superconductivity-induced self-energy evolution of the nodal electron of optimally doped $Bi_2Sr_2Ca_{0.92}Y_{0.08}Cu_2O_{8+\delta}$. *Phys. Rev. B* **77**, 140504(R) (2008).

26. Anzai, H. et al. A new landscape of multiple dispersion kinks in a high-T_c cuprate superconductor. *Sci. Rep.* **7**, 4830 (2017).

27. Horio, M. et al. D-wave superconducting gap observed in protect-annealed electron-doped cuprate superconductors $Pr_{1.3-x}La_{0.7}Ce_xO_4$. *Phys. Rev. B* **100**, 054517 (2019).

28. Santander-Syro, A. F. et al. Two-Fermi-surface superconducting state and a nodal d-wave energy gap of the electron-doped $Sm_{1.85}Ce_{0.15}CuO_4$ cuprate superconductor. *Phys. Rev. Lett.* **106**, 197002 (2011).

29. Sato, T., Kamiyama, T., Takahashi, T., Kurahashi, K. & Yamada, K. Observation of $d_{x^2-y^2}$-like superconducting gap in an electron-doped high-temperature superconductor. *Science* **291**, 1517–1519 (2001).

30. Valla, T., Fedorov, A. V., Johnson, P. D. & Hulbert, S. L. Many-body effects in angle-resolved photoemission: quasiparticle energy and lifetime of a Mo(110) surface state. *Phys. Rev. Lett.* **83**, 2085–2088 (1999).

31. Gweon, G. H., Zhou, S. Y. & Lanzara, A. Strong influence of phonons on the electron dynamics of $Bi_2Sr_2CaCu_2O_{8+\delta}$. *J. Phys. Chem. Solids* **65**, 1397–1401 (2004).

32. Hofmann, P., Sklyadneva, I. Y., Rienks, E. D. L. & Chulkov, E. V. Electron-phonon coupling at surfaces and interfaces. *N. J. Phys.* **11**, 125005 (2009).

33. Wen, C. H. P. et al. Unveiling the superconducting mechanism of $Ba_{0.51}K_{0.49}BiO_3$. *Phys. Rev. Lett.* **121**, 117002 (2018).

34. Johnson, P. D. et al. Doping and temperature dependence of the mass enhancement observed in the cuprate $Bi_2Sr_2CaCu_2O_{8+\delta}$. *Phys. Rev. Lett.* **87**, 177007 (2001).

35. Jin, K., Butch, N. P., Kirshenbaum, K., Paglione, J. & Greene, R. L. Link between spin fluctuations and electron pairing in copper oxide superconductors. *Nature* **476**, 73–75 (2011).

36. He, Y. et al. Rapid change of superconductivity and electron-phonon coupling through critical doping in Bi-2212. *Science* **362**, 62–65 (2018).

37. Li, H. et al. Coherent organization of electronic correlations as a mechanism to enhance and stabilize high-T_c cuprate superconductivity. *Nat. Commun.* **9**, 26 (2018).

38. Dai, P. et al. The magnetic excitation spectrum and thermodynamics of high-T_c superconductors. *Science* **284**, 1344–1347 (1999).

39. Wilson, S. D. et al. Resonance in the electron-doped high-transition-temperature superconductor $Pr_{0.88}LaCe_{0.12}CuO_{4-\delta}$. *Nature* **442**, 59–62 (2006).

40. Zhao, J. et al. Neutron-spin resonance in the optimally electron-doped superconductor $Nd_{1.85}Ce_{0.15}CuO_{4-\delta}$. *Phys. Rev. Lett.* **99**, 017001 (2007).

41. Armitage, P. et al. Angle-resolved photoemission spectral function analysis of the electron-doped cuprate $Nd_{1.85}Ce_{0.15}CuO_4$. *Phys. Rev. B* **68**, 064517 (2003).

42. Matsui, H. et al. Direct observation of a nonmonotonic $d_{x^2-y^2}$-wave superconducting gap in the electron-doped high-Tc superconductor $Pr_{0.89}LaCe_{0.11}CuO_4$. *Phys. Rev. Lett.* **95**, 017003 (2005).

43. Schachinger, E., Homes, C. C., Lobo, R. P. S. M. & Carbotte, J. P. Multiple bosonic mode coupling in the charge dynamics of the electron-doped superconductor $(Pr_{2-x}Ce_x)CuO_4$. *Phys. Rev. B* **78**, 134522 (2008).

44. Rahlenbeck, M. et al. Raman light scattering study and microstructural analysis of epitaxial films of the electron-doped superconductor $La_{2-x}Ce_xCuO_4$. *Eur. Phys. J. B* **75**, 461–467 (2010).

45. Zhang, J.-H. et al. Phenomenological single-particle Green's function for the pseudogap and superconducting phases of high-T_c cuprates. *Phys. Rev. Res.* **2**, 023398 (2020).

ACKNOWLEDGEMENTS

AUTHOR CONTRIBUTIONS

C.Y.T. and Y.J.S. designed the experiments. Z.F.L. and K.J. grew the thin films, C.Y.T. performed ARPES measurements with the assistance of X.C.G., S.Y.G., Z.C.R., J.Z., Y.B.H., and T.Q. C.Y.T. analyzed the ARPES data with help from Y.G.Z. J.X.Z. and Z.Y.W. provided the theoretical advices. C.Y.T., J.Y.G., and H.D. wrote the manuscripts with help from all the other authors. K.J., Y.J.S., and H.D. supervised the project. C.Y.T. and Z.F.L. contributed equally to this work.

COMPETING INTERESTS

The authors declare no competing interests.

ADDITIONAL INFORMATION